Semiconductor Science and Technology

PAPER

Effect of inhomogeneous Schottky barrier height of SnO_2 nanowires device

To cite this article: Cleber A Amorim *et al* 2018 *Semicond. Sci. Technol.* **33** 055003

View the article online for updates and enhancements.

Related content

- Behavior of temperature dependent electrical properties of Pd/Au Schottky contact to GaN grown on Si substrate by MBE
Varun Singh Nirwal and Koteswara Rao Peta

- Current Transport in Copper Schottky Contacts to *a*-Plane/*c*-Plane n-Type $MoSe_2$
C. K. Sumesh, K. D. Patel, V. M. Pathak et al.

- Spatial inhomogeneity in Schottky barrier height at graphene/MoS2 Schottky junctions
D Tomer, S Rajput and L Li

IOP ebooks™

Bringing you innovative digital publishing with leading voices to create your essential collection of books in STEM research.

Start exploring the collection - download the first chapter of every title for free.

This content was downloaded from IP address 200.133.225.27 on 21/09/2018 at 18:45

IOP Publishing Semiconductor Science and Technology

Semicond. Sci. Technol. 33 (2018) 055003 (7pp) https://doi.org/10.1088/1361-6641/aab69e

Effect of inhomogeneous Schottky barrier height of SnO_2 nanowires device

Cleber A Amorim[1], Eric P Bernardo[2], Edson R Leite[3] and Adenilson J Chiquito[2]

[1] Faculdade de Ciências e Engenharia, Universidade do Estado de São Paulo, Campus Tupã, CEP 17602-496, Brazil
[2] NanoLab, Departamento de Física, Universidade Federal de São Carlos—UFSCar, Rodovia Washington Luiz, Km 235 Monjolinho, CP 676, CEP 13565-905, São Carlos, São Paulo, Brazil
[3] LIEC, Departamento de Química, Universidade Federal de São Carlos—UFSCar, Rodovia Washington Luiz, Km 235 Monjolinho, CEP 13565-905, São Carlos, São Paulo, Brazil

E-mail: cleber@tupa.unesp.br

Received 19 January 2018, revised 2 March 2018
Accepted for publication 14 March 2018
Published 4 April 2018

Abstract

The current–voltage (*I–V*) characteristics of metal–semiconductor junction (Au–Ni/SnO_2/Au–Ni) Schottky barrier in SnO_2 nanowires were investigated over a wide temperature range. By using the Schottky–Mott model, the zero bias barrier height Φ_B was estimated from *I–V* characteristics, and it was found to increase with increasing temperature; on the other hand the ideality factor (n) was found to decrease with increasing temperature. The variation in the Schottky barrier and n was attributed to the spatial inhomogeneity of the Schottky barrier height. The experimental *I–V* characteristics exhibited a Gaussian distribution having mean barrier heights $\overline{\Phi}_B$ of 0.30 eV and standard deviation σ_s of 60 meV. Additionally, the Richardson modified constant was obtained to be 70 A cm^{-2} K^{-2}, leading to an effective mass of $0.58m_0$. Consequently, the temperature dependence of *I–V* characteristics of the SnO_2 nanowire devices can be successfully explained on the Schottky–Mott theory framework taking into account a Gaussian distribution of barrier heights.

Keywords: tin oxide, nanowire, gaussian ditribution

(Some figures may appear in colour only in the online journal)

1. Introduction

Over the past decades nanowires have been attracted great interest, due to their high potencial for applications such as ligth emitting diodes [1, 2], gas sensors [3], electroluminescent devices [4] and field effect transistors [5–7]. These electronic devices present smooth control over the flow of charge carriers which are injected into the semiconducting material through electrical contacts. In order to obtain detailed information on structural and electronic properties the study of nanowires based devices could be a useful way to explore these properties and the large dependence of electrical characteristics on surface states.

Kovtyukhova *et al* studied metallic nanowires in which the rectifier character was explained by both Schottky and Fowler–Nordeheim theory [8]. Subsequently, Jae-Ryong Jin *et al* have obtained gallium nitride nanowires grown by chemical vapor deposition, which exhibited Schottky diode behavior [9]. Park and Gyu-Chul presented a study of nanowires of zinc oxide with Schottky nanocontacts. In that paper the authors analyzed the metal–semiconductor junction between a nanowire and Au/ZnO electrodes and an AFM tip used as an electrode. The results showed an operating voltage of 1.0 V and breakdown voltage of −8.0 V.

Ideal Schottky devices have ideality factors close to unity, but in general, values greater than unity are usually observed characterizing these devices as poor quality metal-semiconductor junctions. Electrical contacts having Schottky barrier with $n > 1$ have been studied by Kim *et al* and Lao *et al* [9, 10]. Nevertheless few authors try to explain the reasons for high ideality factor values which are found in nanowire devices [11]. Usually, the ideality factor greater

 © 2018 IOP Publishing Ltd Printed in the UK

than unity can be attributed to interface states in a thin oxide layer between the metal and semiconductor and/or due to tunneling currents in highly doped semiconductors [9, 11–13]. Other authors have highlighted the image charge effect or recombination/generation within the space charge region as a mechanism responsible for $n > 1$ [14, 15].

All studies presented in the previous paragraph take into account that the device behaves as an ideal Schottky diode, assuming that the junction is abrupt with a well defined Schottky barrier height (SBH). Also, some authors have attributed the deviations from ideality factor to presence of a non-homogeneous SBH [15–17]. Both Pipinys and Lapeika as well as Gayen *et al* found ideality factors above unity and SBHs dependent on both temperature and voltage. This fact is not predicted by the thermionic emission model [18, 19].

In this work we studied devices based on nanowires which exhibited some inhomogeneity on the SBH. This inhomogeneity led to a temperature dependence of devices parameteres such as SBH and ideality factor which is not predicted in the Schottky–Mott model. Such variation in both SBH and n can be explained in assumption of a spatial inhomogeneity of the SBH. Here we used the Schottky–Mott theory framework assuming a Gaussian distribution and parameters such as standard deviation, mean Schottky barrier heigth and an apparent ideality factor were obtained. In addition, the modified Richardson constant was also obtained and the electron effective mass of SnO_2 was estimated.

2. Materials and methods

Tin oxide (SnO_2) nanowires were synthesized by a carbothermal evaporation using the well known vapor solid mechanism; the tin source was the SnO_2 powder (Aldrich, >325 mesh, purity >99.9%) which was mixed with graphite (Aldrich, >20 μm, purity >99%) 95:5 in weight, respectively, by using a balls mill for 24 h. The obtained mixture was put in a crucible and then it was placed at the center of a horizontal tube furnace (Lindberg Blue M), where the temperature, gas flux and evaporation time were controlled in order to obtain the best conditions for the synthesis. From room temperature to 600 °C an inert atmosphere was used, keeping a 100 SCCM N_2 flow. From 600 °C to the end of the synthesis time, a controlled O_2 quantity was admitted in both tube extremities. The synthesis was carried out at 1200 °C for 2 h, using a 10 °C min^{-1} as heating rate. The white material collected after the synthesis was structurally and electrically characterized. The material structure was analyzed by x-ray diffraction (XRD) using a Rigaku diffractometer model DMAX 2500PC, with Cu-Kα radiation ($\lambda = 1.540\,56$ Å) at 40 kV and 150 mA. A scanning electron microscope (SEM) FEI INSPECT F50 was used for microanalysis (EDX) and microstructure characterization. Single SnO_2 nanowire devices were prepared by a conventional random dispersion technique and ohmic contacts were made by conventional photolitography producing electrodes with spacing of 10 μm. These devices were used to investigated the temperature dependence of resistivity (indium electrode, ohmic behavior) and current–voltage characteristic. Schottky parameters were also investigated using gold–nickel alloy electrodes. The transport measurements were carried out at different temperatures from 10 to 300 K using a closed cycle helium cryostat at pressures lower than 5×10^{-6} mbar. Temperature-dependent resistivity was measured using standard low-frequency lock-in techniques ($f = 13$ Hz) using a Keithley 6221 as a current source. The current–voltage curves at different temperatures were obtained by using a Keithley 6517 electrometer.

3. Experimental results and discussion

Figure 1 depicts the structural properties of the as-grown SnO_2 nanobelts. Panel (a) presents the XRD pattern of SnO_2 nanobelts. Some information on the preferential growth direction of samples can be obtained by the intensity ratio of the (100) and (101) reflections when compared with the standard JCPDF card [20], due to the large aspect ratio of morphology of the samples (belts), with a ratio $\frac{I_{110}}{I_{101}} = 1.11$. Figure 1(b) presents a SEM image of the collected material showing an abundant and uniform growth of nanobelts with lateral sizes between 5 and 500 nm and lengths of tens of micrometers. The chemical characterization of several nanobelts was made using an Energy Dispersive x-ray spectrometer attached to a SEM, where the presence of Sn and O is observed. The peak related to Si is due to the substrate used (figure 1(c)). Corroborating the previous analysis, Raman spectrum of the as-grown material showed that the samples are structurally uniform and present the rutile structure, belonging to the space group $P_{42/mnm}$, where the normal modes of vibration are in the center of Brillouin zone [21–23] with 11 Raman-active optical phonons [24] (figure 1(d)). Concomitantly, the tetragonal rutile structure of SnO_2 samples was confirmed with the presence of the E_g, A_{1g} and B_2 modes. It is also possible to observe the presence of two additional peaks at 501 and 690 cm^{-1} which are not frequentelly observed in the bulk type samples. Berengue *et al* related the presence of these peaks in the SnO_2 nanostructured with different selections rules due to a structural disorder or low dimensionality of the samples [25].

The temperature-dependent resistance is plotted in figure 2(a). From these results the transport characteristics of the SnO_2 nanobelts studied here are in agreement with a semiconductor behavior. Figure 2(b) presents a scanning electron microscopy image of the device used for the temperature-dependent resistance measurements. The lateral dimensions of the nanobelt showed in figure 2(b) are of the order of tens of nanometers and a length of a few micrometers. It is important to emphasize, as widely referred in the literature that both donor defects and oxygen vacancies are capable of producing electrons within the conduction band, because positive charged states are favorable for Fermi energies over the whole band gap which could participate in the current transport [26–28]. Indeed, vacancies induce disorder in the electronic spectrum leading to a certain degree of

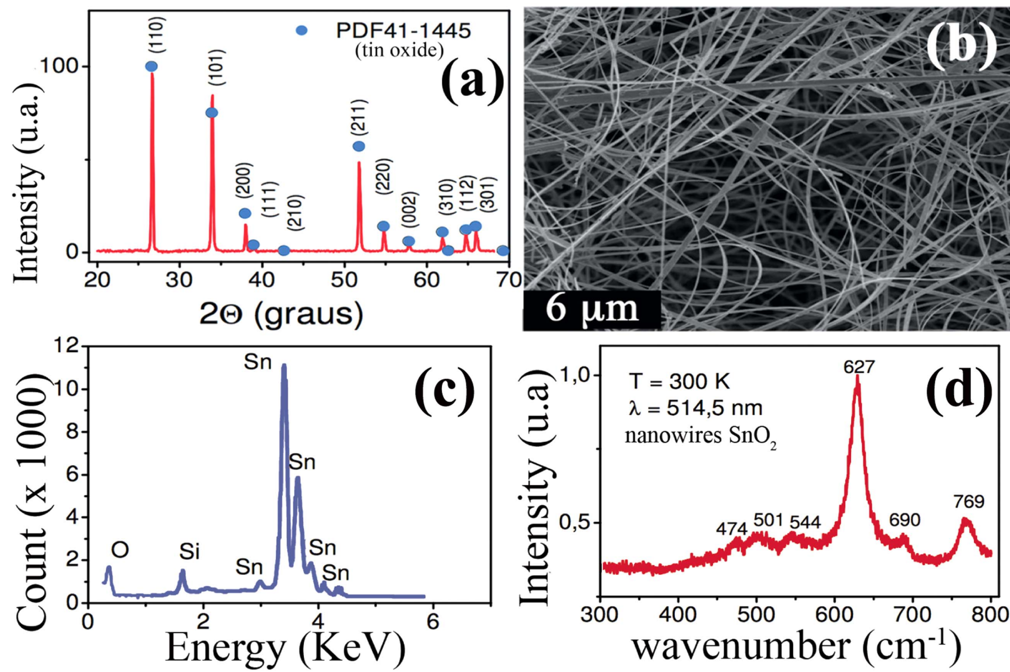

Figure 1. Panel (a) presents the x-ray diffraction (XRD) pattern of SnO_2 nanobelts, the data was analyzed following the PDF 41-1445 card. (b) The SEM characterization of the as-grown nanobelts showing the VS character of the growth and morphology of the nanobelts. (c) EDX spectrum used to quantify the chemical composition of the samples and (d) Raman data show the tin oxide (rutile structure) fingerprint: 474, 501, 544, 627, 690 and 769 cm^{-1} modes.

carriers localization at low temperatures. Figure 2(c) shows that the VRH model fits well the resistance data in the temperature range $60 < T < 300$ K (straight line in figure 2(c)). This mechanism, which is also valid in a three-dimensional case, is described by equation [29],

$$\rho(T) = \rho_0 \exp\left[\left(\frac{T_0}{T}\right)^m\right], \quad (1)$$

where $T_0 = 5.7\alpha^{-3}/k_B N(E_F)$, $m = 1/(d+1)$, and d is the system dimensionality. Here $N(E_F)$ is the density of states at the Fermi level and (α^{-1}) is the localization length.

The model based on the thermal activation law or Efros VRH mechanism was unable to explain the observed behavior because some physical parameters, such as localization length or excitation energy, invariably assume unreasonable values. The fitting of equation (1) to the experimental data revealed that the mechanism transport is mainly governed by the VRH process. The fitting of low dimensional hopping laws ($m = 1/3$ and $m = 1/2$) were also performed but was discarded due to the poor agreement between these mechanism and the experimental data. Also, the fitting procedure by means of equation (1) provided $T_0 = 13\ K^{1/4}$, and the value found in the literature was $T_0 = 4\ K^{1/4}$ [30]. By considering the density of states, $N(E_F) = 10^{20}\ eV^{-1}\ cm^{-3}$ the localization length of samples was estimated to be 5 nm [31, 32]. This value is in according with radius Bohr of SnO_2 (3.3 nm). In addition, from the VRH fitting it was found the hoping distance to be 7.7 nm at room temperature, which is much smaller than the cross section of nanobelts ($\sim 500 \times 50\ nm^2$) emphasizing that the samples have a three-dimensional nature.

The knowledge of parameters such as SBH, surface states, contact resistance, ideality factor, Richardson constant, etc plays a fundamental role for the characterization and understanding of metal-semiconductor junction behavior. Aiming the study of these parameters a single SnO_2 nanobelt device was built using gold–nickel alloy (Au–Ni) as electrical contacts, forming a Schottky barrier of 0.25 eV according to the Schottky–Mott theory [33].

Figure 3(a) shows the current–voltage characterization at different temperatures revealing the formation of a double potential barrier, as expected, since the electrical contacts are identical for both interfaces. Furthermore, the symmetry observed in both polarities shows the quality of the contacts presenting barriers characterized by very close values. Figure 3(b) shows the ideality factor versus reciprocal temperature and SBH-temperature dependence; however, according to the model presented by Schottky–Mott, both ideality factor and the barrier height should be temperature independent. Also, thermionic emission theory predicts a ideality factor very close to the unit. Zeyrek *et al*, showed that in a thermally activated process, electrons at low temperatures are not able to jump much higher barriers than $k_B T/e$, which makes the ideality factor different from unit. As the temperature increases, more electrons have enough energy to overcome the barrier and as a result the barrier height appears to increase with increasing temperature and the applied voltage [34].

Figure 3(c) presents Richardson plots and I_0 values were obtained by extrapolating the fitting curves to the current axis (figure 3(a)). Plots like those in 3(c) are often used to determine the SBH, but in this case, there is no a single activation

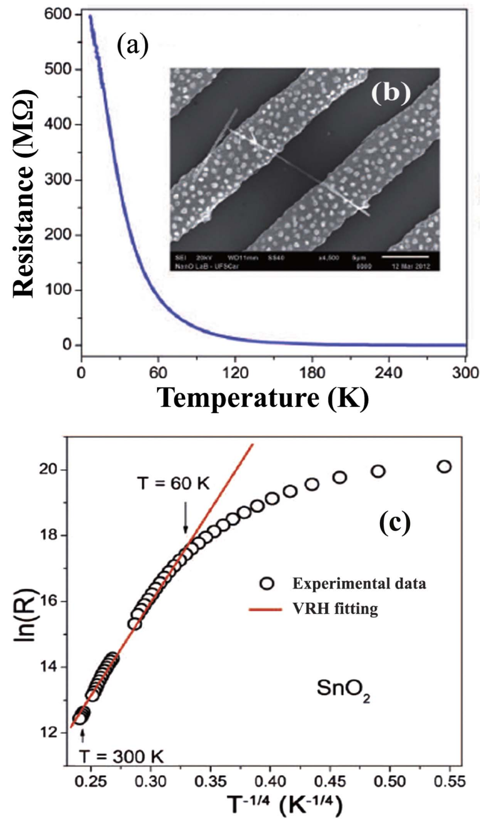

Figure 2. In (a) temperature-dependent resistance measuments of a SnO_2 nanobelt device with indium electrodes are displayed (showed in the inset—(b)). The sample presents a typical semiconductor behavior, since the resistance decreases with increasing temperature in the whole range used for measurements. Painel (c) shows the fitting of the VRH theory to the experimental data.

energy to be extracted out from the plots. According to Mott [33]

$$\ln\left(\frac{I_0}{T^2}\right) = \ln(A^*) - \frac{q\Phi_{B0}}{k_B T} \quad (2)$$

and the activation energy $E_{\rm act}$ can be obtained by

$$E_{\rm act} = k\frac{{\rm d}\left[\ln\left(\frac{I_0}{T^2}\right)\right]}{{\rm d}(1/T)} = -q\Phi_{B0}, \quad (3)$$

if the SBH (Φ_{B0}) is independent of the temperature T: in this case, figure 3(c) should yield a straigh line with $E_{\rm act}$. The curves bending in figure 3(c) demonstrates that there is no a single activation energy.

With decrease SBH increasing temperature, n tend to increase, resulting in a curvature or distortion of the Richardson plot. The curvature of this plot has been reported widely, and in this case the modified version of the Richardson plot is often employed. However, as suggested from figure 3(c), the modified Richardson plot is not always successful in rectifying the curvature observed in the original curves. The deviation in the plots may be due to the spatial inhomogeneities of the barrier height and potential fluctuations at the interface. Therefore, we determine Φ_{B0} directly from the I_0 values using the Mott model and the Richardson constant $A^* = \frac{4\pi e m^* k_B^2}{h^3} = 120\,\frac{m^*}{m_0}$ A cm^{-2} K^{-2}, where m^* is the effective mass and m_0 rest mass.

The temperature dependence of n has been attributed to interface states, and quantum mechanical tunneling barrier due to lowering of the charge image effect by several authors [13, 35–37]. A variation in the homogeneity of the Schottky contact leading to a distribution of barrier heights, as assumed by several authors [38–42], is quite attractive for our case: taking into account that the system is self-organized, inhomogeneities at the surfaces of the samples are unavoidable and this could lead to a random distribution of Schottky barriers.

The barrier inhomogeneity approach mainly assumes that there is a distribution of barrier heights under the rectifying contact. Different types of distribution functions are suggested for describing barrier height inhomogeneities, for example Gaussian [15, 17, 38] and log-normal ones [43]. In order to explain the observed variations in the barrier height and ideality factor, let us assume a Gaussian (random) distribution for the barrier height, as considered by various authors [38–42], with a mean value $\overline{\Phi}_B$ and standard deviation σ_s, which can be written as

$$P(\Phi_B) = \frac{1}{\sigma_s\sqrt{2\pi}}\exp\left[-\frac{(\Phi_B - \overline{\Phi}_B)^2}{2\sigma_s^2}\right], \quad (4)$$

where $1/\sigma_s\sqrt{2}\pi$ is the normalization constant, Φ_B and $\overline{\Phi}_B$ are the SBH and the average barrier, respectively. The total current $I(V)$ across a Schottky diode containing barrier inhomogeneties can be expressed as

$$I(V) = \int_{-\infty}^{\infty} I(\Phi_B, T)P(\Phi_B){\rm d}\Phi_B, \quad (5)$$

where $I(\Phi_B, T)$ is the current at bias V for a barrier height based on the ideal thermionic-emission-diffusion theory and $P(\Phi_B)$ is the normalized distribution function.

In order to use the model proposed by equation (4), several current-voltage measurements (130 in total; $T = 300$ K) have been conducted in Au–Ni/SnO_2/Au–Ni devices and the SBH was obtained according to the Schottky–Mott model equation (2).

Figure 3(d) shows the statistical distribution of the SBH at 300 K. In this case, the distribution can be fitted quite well by a Gaussian function. The value of full width at half maximum is 75 meV, and the standard deviation yield $\sigma_s = 60$ meV. The average SBH is 0.30 eV, higher than predicted by Mott theory (0.25 eV), and very close to that obtained by Chiquito *et al*, which considered the presence of interface states affecting the charge exchange at the metal/semiconductor interface [21].

Solving equation (5) we obtain an expression for the current through the Schottky barrier, similar to Mott model considering a modified barrier. However, as we change temperature and applied voltage, the Schottky barrier Gaussian distribution model allows both SBH and idealtiy factors values to be variables of the system [39–42] as described in

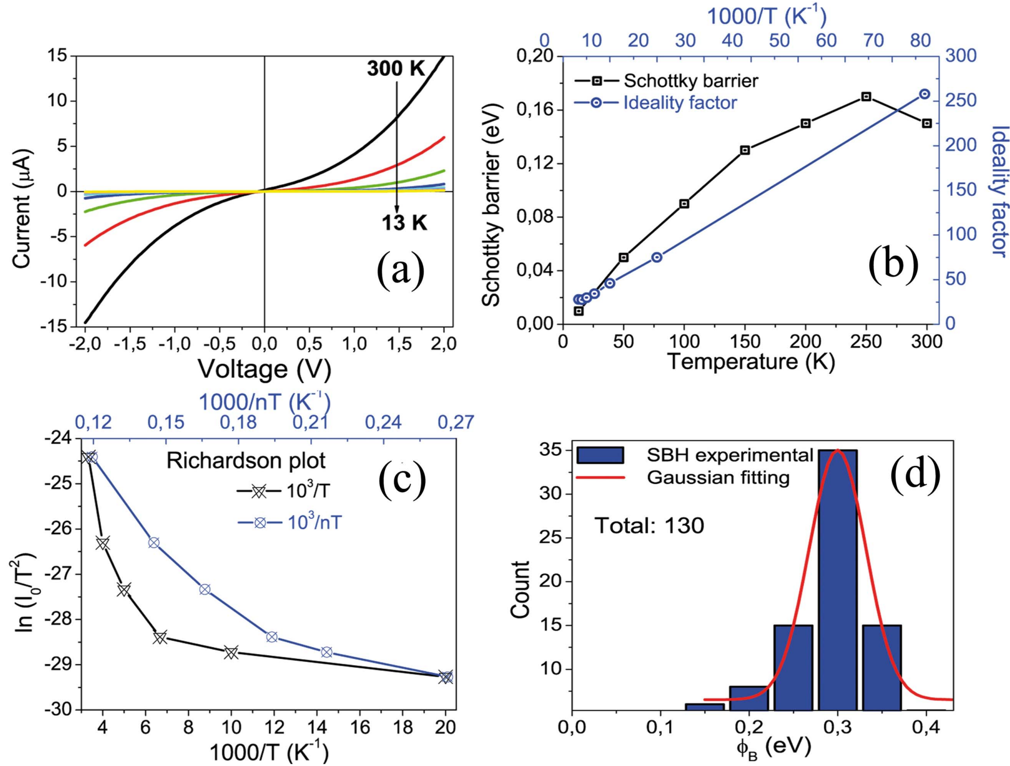

Figure 3. In (a) current–voltage curves taken at different temperatures are displayed; (b) ideality factor versus reciprocal temperature and Schottky barrier height-temperature dependence are showed for Au–Ni/SnO_2/Au–Ni device; (c) the nonlinear nature of Richardson plots, $\ln(I_0/T^2)$ versus $1000/T$ and $\ln(I_0/T^2)$ versus $1000/nT$ and (d) Schottky barrier distribution. 130 measurements were used to raise this curve.

the following equation:

$$I(V) = SA^{**}T^2 \exp\left(\frac{-e\phi_{\text{ap}}}{k_B T}\right)\exp\left[\left(\frac{eV}{n_{\text{ap}}k_B T}\right) - 1\right], \quad (6)$$

where ϕ_{ap} (representing an apparent barrier height) is given by

$$\Phi_{\text{ap}} = \overline{\Phi}_{B0}(T=0) - \frac{\sigma_{s0}^2}{2k_B T} + \alpha T, \quad (7)$$

and the apparent ideality factor is

$$\left(\frac{1}{n_{\text{ap}}} - 1\right) = \rho_1 - \frac{q\rho_2}{2k_B T}, \quad (8)$$

where σ_{s0} is the standard deviation at $V = 0$, α is the SBH temperature coefficient, ρ_1 and ρ_2 are voltage coefficients. The coefficients ρ_1 and ρ_2, may depend on temperature, quantifying the voltage deformation of the barrier height distribution [44].

Here it was assumed that the mean SBH and σ_s are linearly bias-dependent on Gaussian parameters, such as $\overline{\Phi}_B = \overline{\Phi}_{B0}(T=0) + \rho_2 V$ and deviation $\sigma_s = \sigma_{s0} + \rho_3 V$, where $\rho_2 V$ and $\rho_3 V$ voltage coefficients, which may depend on temperature, quantifying the deformation on the SBH distribution [44]. It is clear that the barrier height is a consequence of the existence of the Gaussian distribution and its influence is determined by the standard deviation itself, ϕ_{ap} and n_{ap}. Thus, the plot ϕ_{ap} versus $q/2k_B T$ (figure 4(a)) should be a straight line that gives $\overline{\Phi}_{B0}(T=0) = 124$ meV and $\sigma_{s0} = 69$ meV from the x-axis intercept and slope, respectively.

The linear behavior of figure 4(b) demonstrates that the ideality factor express the deformation of the Gaussian distribution of the SBH. In accordance to the results the inhomogeneity and potential fluctuation are dramatically affected by low temperature current- voltage characteristics. It is responsible for the curved behavior in the Richardson plot in figure 3(c).

Now, the Richardson plot is modified by combining equations (6) and (7) as follows

$$\ln\left(\frac{I_0}{T^2}\right) - \left(\frac{q^2\sigma_0^2}{2k_B^2 T^2}\right) = \ln(AA^*) - \frac{\overline{\Phi}_{B0}}{k_B T}. \quad (9)$$

Figure 4(c) shows de Richardson modified plot and according to equation (8) should be a straight line with the slope directly yielding the mean $\overline{\Phi}_{B0}$ and the intercept [$=\ln(AA^*)$] determining A^* for a given diode area A (equation inserted in figure 4(c)). From Richardson modified plot we obtained $\overline{\Phi}_{B0}$ and A^* as 0.42 eV and 70 A cm^{-2} K^{-2}, respectively, without using the temperature coefficient of SBHs. The value of the Richardson constant corresponds to the effective mass of $0.58m_0$, with m_0 being the electron rest mass; this value is in according with reported in the literature by Sanon *et al* [45].

Therefore it is reasonable to assume that the irregularities on the surface, devices based on nanowires present a

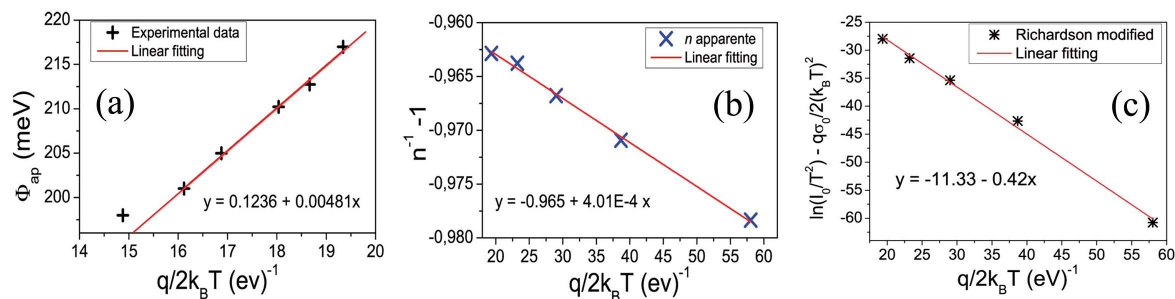

Figure 4. (a) The zero-bias apparent barrier plot and (b) ideality factor for Au–Ni/SnO_2/Au–Ni device according to Gaussian distribution and (c) temperature dependence of modified Richardson for Au–Ni/SnO_2/Au–Ni device according to Gaussian distribution.

inhomogeneity in the SBH. This inhomogeneity implies in SBH and n temperature dependence, which is not predicted by the Schottky–Mott model. Chand and Kumar [46] assumed a random distribution of SBH determining it with a standard deviation (associating these parameters to imperfections in the metal–semiconductor junction). Furthermore, this assumption allows an interpretation of the dependence of SBH and ideality factor on temperature as seen in figures 4(a), (b).

4. Conclusion

Current–voltage characteristics of Au–Ni/SnO_2/Au–Ni devices were measured in a wide temperature range. The experimental results showed the non-ideal behavior of the current-transport over the barrier expressed by ideality factor significantly larger than unity at lower temperatures and an increasingly SBH as the temperature increases. The high value of n is attributed to interface states, and quantum mechanical tunneling barrier due to lowering of the charge image effect. In order to obtain evidences of a random distribution of the SBHs, we have raised the $\overline{\Phi}_{ap}$ versus $q/2k_BT$, and as result, a straight line with positive slope for Gaussian distribution of SBHs was observed. The slope of the fitting data gives the standard deviation and the intercept at the ordinate yields the mean SBH. We obtained the modified Richardson constant $A^* = 70$ A cm^{-2} K^2. From these results, the I–V–T characteristics of Au–Ni/SnO_2/Au–Ni devices can be satisfactorily explained on the basis of the thermionic emission mechanism with a single Gaussian distribution of the SBHs.

Acknowledgments

The authors thank the Brazilian research funding agencies FAPESP (FAPESP 2014/19692-4) and CNPq (305615/2014-0) for the financial support of this work.

ORCID iDs

Cleber A Amorim https://orcid.org/0000-0003-4123-2740

References

[1] Konenkamp R, Word R C and Schlegel C 2004 *Appl. Phys. Lett.* **85** 6004
[2] Min K W, Kim Y K, Shin G, Jang S, Han M, Huh J, Kim G T and Ha J S 2011 *Adv. Funct. Mater.* **21** 119
[3] Patolsky F, Zheng G and Lieber C M 2006 *Anal. Chem.* **78** 4260
[4] Mazzera M, Zha M, Calestani D, Zappettini A, Lazzarini L, Salviati G and Zanotti L 2007 *Nanotechnology* **18** 355707
[5] Greytak A B, Lauhon L J, Gudiksen M S and Lieber C M 2004 *Appl. Phys. Lett.* **84** 4176
[6] Colinge J-P, Lee C-W, Afzalian A, Akhavan N D, Yan R, Ferain I, Razavi P, O'Neill B and Blake, M A 2010 *Nat. Nanotechnol.* **5** 225
[7] Fan Z, Wang D, Chang P C, Tseng W Y and Lu J G 2004 *Appl. Phys. Lett.* **85** 5923
[8] Kovtyukhova N I, Martin B R, Mbindyo J K, Smith P A, Razavi B, Mayer T S and Mallouk T E 2001 *J. Phys. Chem.* B **105** 8762
[9] Kim J-R, Oh H, So H M, Kim J-J, Kim J, Lee C J and Lyu S C 2002 *Nanotechnology* **13** 701
[10] Lao C S, Liu J, Gao P, Zhang L, Davidovic D, Tummala R and Wang Z L 2006 *Nano Lett.* **6** 263
[11] Woodruff S, Dellas N, Liu B, Eichfeld S, Mayer T, Redwing J and Mohney S 2008 *J. Vac. Sci. Technol.* B **26** 1592
[12] Card H and Rhoderick E 1971 *J. Phys. D: Appl. Phys.* **4** 1589
[13] Rhoderick E H and Williams R H 1988 *Metal-Semiconductor Contacts* vol 129 (Oxford: Clarendon) (https://doi.org/10.1049/ip-i-1.1982.0001)
[14] Rideout V and Crowell C 1970 *Solid-State Electron.* **13** 993
[15] Werner J H and Güttler H H 1991 *J. Appl. Phys.* **69** 1522
[16] Song Y, Van Meirhaeghe R, Laflere W and Cardon F 1986 *Solid-State Electron.* **29** 633
[17] McCafferty P, Sellai A, Dawson P and Elabd H 1996 *Solid-State Electron.* **39** 583
[18] Gayen R, Bhattacharyya S and Jana P 2014 *Semicond. Sci. Technol.* **29** 095022
[19] Pipinys P and Lapeika V 2010 *Adv. Condens. Matter Phys.* **2010** 526929
[20] Law M, Kind H, Messer B, Kim F and Yang P 2002 *Angew. Chem.* **114** 2511
[21] Chiquito A J, Amorim C A, Berengue O M, Araujo L S, Bernardo E P and Leite E R 2012 *J. Phys.: Condens. Matter* **24** 225303
[22] Zhou J, Zhang M, Hong J and Yin Z 2006 *Solid State Commun.* **138** 242
[23] Sun S, Meng G, Zhang M, An X, Wu G and Zhang L 2004 *J. Phys. D: Appl. Phys.* **37** 409
[24] Scott J 1970 *J. Chem. Phys.* **53** 852

[25] Berengue O M, Simon R A, Chiquito A J, Dalmaschio C J, Leite E R, Guerreiro H A and Guimarães F E G 2010 *J. Appl. Phys.* **107** 033717
[26] Berengue O, Amorim C, Kamimura H, Chiquito A and Leite E 2012 *J. Appl. Phys.* **111** 013713
[27] goston P A, Erhart P, Klein A and Albe K 2009 *J. Phys.: Condens. Matter* **21** 455801
[28] Zheng M, Zhang L-D, Li G-H, Zhang X and Wang X 2001 *Appl. Phys. Lett.* **79** 839
[29] Shklovskii B, Levin E, Fritzsche H and Baranovskii S D 1990 *Adv. Disord. Semicond.* **3** 161
[30] Sato T, Ohashi K, Sugai H, Sumi T, Haruna K, Maeta H, Matsumoto N and Otsuka H 2000 *Phys. Rev.* B **61** 12970
[31] Giraldi T R, Escote M T, Maciel A P, Longo E, Leite E R and Varela J A 2006 *Thin Solid Films* **515** 2678
[32] Aouaj M A, Diaz R, Belayachi A, Rueda F and Abd-Lefdil M 2009 *Mater. Res. Bull.* **44** 1458
[33] Mott N 1968 *Rev. Mod. Phys.* **40** 677
[34] Zeyrek S, Altindal S, Yuzer H and Bulbul M 2006 *Appl. Surf. Sci.* **252** 2999
[35] Crowell C 1977 *Solid-State Electron.* **20** 171
[36] Tung R, Levi A, Sullivan J and Schrey F 1991 *Phys. Rev. Lett.* **66** 72
[37] Chand S and Kumar J 1995 *Semicond. Sci. Technol.* **10** 1680
[38] Chand S and Kumar J 1996 *Semicond. Sci. Technol.* **11** 1203
[39] Özdemir A F, Turut A and Kökçe A 2006 *Semicond. Sci. Technol.* **21** 298
[40] Zeng J-J and Lin Y-J 2014 *Appl. Phys. Lett.* **104** 133506
[41] Das A, Kushwaha A, Sivasayan R K, Chakraborty S, Dutta H S, Karmakar A, Chattopadhyay S, Chi D and Dalapati G K 2016 *J. Phys. D: Appl. Phys.* **49** 145105
[42] Chand S 2003 *Semicond. Sci. Technol.* **19** 82
[43] Horvath Z J 1992 *MRS Proc.* **260** 441
[44] Korucu D and Duman S 2013 *Thin Solid. Films* **531** 436
[45] Sanon G, Rup R and Mansing A 1993 *Phys. Status Solidi* a **135** 581
[46] Chand S and Kumar J 1997 *J. Appl. Phys.* **82** 5005